ACS APPLIED ENERGY MATERIALS

www.acsaem.org Article

Revealing the Interfacial Photoreduction of MoO_3 with P3HT from the Molecular Weight-Dependent "Burn-In" Degradation of P3HT:$PC_{61}BM$ Solar Cells

Huimin Gu, Lingpeng Yan, Sonam Saxena, Xueliang Shi, Xuning Zhang, Zerui Li, Qun Luo, Huiqiong Zhou, Yongzhen Yang,* Xuguang Liu, Wallace W. H. Wong, and Chang-Qi Ma*

Cite This: *ACS Appl. Energy Mater.* 2020, 3, 9714–9723 Read Online

ACCESS | Metrics & More | Article Recommendations | Supporting Information

ABSTRACT: "Burn-in" degradation occurs in many polymer solar cells, which dramatically reduces the overall power output of the cells at the early hundred hours. Understanding the "burn-in" degradation mechanism is therefore highly important to improve the lifetime of the cell. In this article, the decay behaviors of P3HT:$PC_{61}BM$ solar cells depending on the molecular weight of P3HT were systematically investigated. Although all of these P3HTs were highly crystalline with regioregularity of 94–97%, the stability of P3HT:$PC_{61}BM$ cells showed a nonmonotonic dependence on P3HT molecular weight. The cells based on P3HT with a weight average molecular weight (M_w) of 20 K showed much faster decadence in open circuit voltage (V_{OC}) and fill factor (FF) during aging, yielding the lowest stability in comparison with that based on P3HT of 10, 25, and 30 K. UV–vis absorption and external quantum efficiency spectra demonstrated that the performance decay is not attributed to the change in the photoactive layer. The recovery of V_{OC} and FF of the aged cells after renewing the MoO_3/Al electrode revealed that the performance decay is mainly because of the interfacial degradation of P3HT:$PC_{61}BM$/MoO_3. Electron spin resonance spectroscopy and X-ray photoelectronic spectroscopy confirmed the photon-induced redox reaction between P3HT and MoO_3 under light illumination, where P3HT is oxidized to the polaron and Mo(VI) was partially reduced to Mo(V). The photon chemical reduction (PCR) of MoO_3 by P3HT is then ascribed as the essential reason for the fast V_{OC} and FF decays of the cells during aging. The surface morphology of the photoactive layer measured by the atomic force microscope revealed the much rougher surface of the P3HT-20 K/$PC_{61}BM$ film. Such a rough surface increases the contact area between P3HT and MoO_3, and consequently enhances the PCR of MoO_3 and P3HT, which is considered as the main reason for the molecular weight-dependent degradation behaviors. For the first time, the current work clearly demonstrates that the photoreduction of the metal oxide and photoactive layer would lead to fast V_{OC} and FF decays, which could be a very important degradation pathway for polymer solar cells.

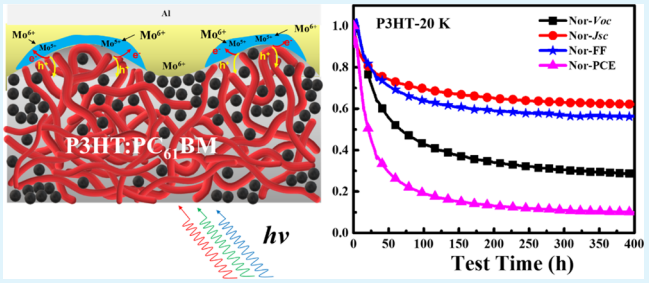

KEYWORDS: *polymer solar cells, stability, "burn-in" degradation, interface decay, photon chemical reduction, surface morphology*

INTRODUCTION

Conjugated polymer-based solar cells, also named as bulk-heterojunction solar cells, have attracted widespread attention in the last few years owing to their advantages of flexibility, lightweight, and excellent compatibility with printing processing.[1−3] High power conversion efficiencies (PCE) of more than 16[4−6] and 17%[7] were reported for the single and tandem junction cells, demonstrating excellent application prospects for the next future. Although a few papers are reporting the stable polymer solar cells with an operation lifetime of 7−10 years,[8−10] statistical data revealed that the stability of polymer solar cells is far from satisfactory.[11] Understanding the degradation mechanism and improving the operation lifetime of polymer solar cells have become the next key challenges for polymer solar cells before commercialization.

It is known that most of the polymer/fullerene solar cells suffer a fast "burn-in" degradation, which dramatically reduces the overall power output of the cells at the first hundred hours.[12,13] Recent works have demonstrated that photon-dimerization of $PC_{61}BM$ is one of the main reasons for the "burn-in" degradation of polymer/fullerene solar cells.[14−16] For example, Brabec *et al.*[17] demonstrated that relatively pure donor and acceptor domains formed within the photoactive

Received: June 7, 2020
Accepted: September 21, 2020
Published: September 21, 2020

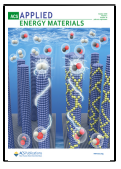

https://dx.doi.org/10.1021/acsaem.0c01325
ACS Appl. Energy Mater. 2020, 3, 9714–9723

layer for crystalline polymers, which reduces the charge recombination and makes this type of cell insensitive to energetic disorder. Therefore, open-circuit voltage (V_{OC}) of the crystalline polymer-based cells is stable during aging. However, pure electron acceptor domains formed in this type of cells promotes the photon dimerization of fullerene molecules and consequently leads to fast short circuit current (J_{SC}) decay.[15] In contrast, for amorphous conjugated polymers, donor and acceptor molecules are well-intermixed in the blend film, making this type of cell sensitive to energetic disorder but insensitive to the photon dimerization of fullerenes. Therefore, fast V_{OC} decay and rather stable J_{SC} are typically found for the amorphous polymer-based cells.[17,18] Our recent work also demonstrated that the fast J_{SC} decay of polymer/fullerene solar cells are directly correlated with the external load attached to the cells during aging, that is, to the concentration of high energy excitons within the blend film.[16] Very recently, Brabec et al. demonstrated that spinodal donor−acceptor demixing also led to fast J_{SC} decay in polymer/fullerene solar cells,[19] which is considered as the third rapid degradation pathway to the polymer/fullerene solar cells.

In addition to the photoactive layer, interfacial layers may also influence device performance and stability. For example, McGehee *et al.* found that a thin conjugated polymer layer formed during aging under the top electrode and acted as a barrier layer for charge extraction that degrades the V_{OC} of the cell under high operating temperature.[20] Zhou *et al.* demonstrated that the UV light-induced decomposition of the nonfullerene acceptor by ZnO led to poor performance stability,[21] which could be improved by using the UV-light inert SnO_2 layer. Later Park and Son also reported the intrinsic photodegradation of polymer solar cells caused by UV-light-induced decomposition of the nonfullerene acceptor component.[22] Our recent results proved that the degradation at the photoactive layer and MoO_3 interface is the main reason for V_{OC} and fill factor (FF) decays of P3HT/fullerene bis-adducts solar cells.[23] However, there is no other interfacial degradation mechanism reported in the literature for polymer solar cells under operation.

From the molecular structure point of view, regioregularity[24,25] and molecular weight[26,27] are key parameters defining conjugated polymers for the application in solar cells. Both factors can influence the performance and stability of polymer solar cells. Although the influence of the molecular weight on photovoltaic performance has been reported,[28−30] there is no paper discussing the impact of molecular weight on device stability. Understanding this will help understand the specific degradation behaviors of polymer solar cells, and will guide the optimization of polymers for use in polymer solar cells. In this work, we systematically investigated the influence of the molecular weight of P3HT on the "burn-in" degradation behavior of P3HT:$PC_{61}BM$ solar cells. Results indicated that the stability of P3HT:$PC_{61}BM$ cells was not monotonously dependent on the molecular weight of P3HT. P3HT-20 K showed the lowest device stability, while the polymers with higher or lower molecular weight (10, 25, 30 K) showed better device stability. For P3HT-20 K-based cells, V_{OC} and FF decays dominate the overall performance loss. Spectroscopic studies confirmed that the photon-chemical reduction (PCR) of MoO_3 by P3HT occurred during aging, which was ascribed to be the main reason for the fast V_{OC} and FF "burn-in" decays. Surface morphology analyses revealed that the rougher surface of P3HT-20 K/$PC_{61}BM$ films increased the interaction between P3HT and MoO_3, and then induced the poorer device stability of the P3HT-20 K-based cells. These results demonstrate that the interface photon-chemical reaction has a significant influence on the stability of polymer solar cells, and a smoother surface could help achieve higher device stability.

EXPERIMENT PART

Materials. Regioregular poly(3-hexylthiophene-2,5-diyl)s (P3HT-10 K, M_w = 1.16 × 10^4 g/mol, Đ (dispersity) = 1.15, regioregularity Rr = 94.3%; P3HT-20 K, M_w = 2.12 × 10^4 g/mol, Đ = 1.11, regioregularity Rr = 96.1%; P3HT-25 K, M_w = 2.64 × 10^4 g/mol, Đ = 1.40, regioregularity Rr = 97.1%; P3HT-30 K, M_w = 3.05 × 10^4 g/mol, Đ = 1.37, regioregularity Rr = 97.1%) were synthesized by a Ni-catalyzed metathesis coupling reaction according to the literature.[31] [6,6]-Phenyl-C_{61}-butyric acid methyl ester ($PC_{61}BM$) was purchased from Solenne B.V. Molybdenum oxide (MoO_3) was purchased from Strem Chemicals, Inc., America. Sodium hydroxide (NaOH) was purchased from Sinopharm Chemical Reagent Co. Ltd., China. All materials were used as received. Zinc oxide nanoparticles (ZnO) were prepared through the reaction of KOH and $Zn(OAc)_2$ in methanol solvent as reported by Beek *et al.*[32]

Method for Solar Cell Fabrication. The devices were fabricated from patterned ITO glass (Shenzhen Southern China City Hunan Technology Co. Ltd.). The substrates were sequentially sonically cleaned in detergent, deionized water, acetone, and isopropanol, and finally treated in a UV−ozone oven for 30 min. First, filtered ZnO (12 mg/mL in methanol) was spin-coated on ITO substrates at 2000 rpm for 60 s. Then, the samples were annealed at 130 °C for 10 min on a hot plate. A blend solution of P3HT and $PC_{61}BM$ in ortho-dichlorobenzene [1:1 (w/w), 40 mg/mL] was spin-coated on the top of the ZnO layer at 600 rpm for 60 s. The wet P3HT:$PC_{61}BM$ blend films were then put into covered petri dishes for 1.5 h[16] The samples were subsequently heated at 125 °C for 10 min. Finally, MoO_3 (10 nm) and Al (100 nm) were sequentially vacuum deposited on the top of the active layer as the hole-extraction layer and anode, respectively. The size of the substrate was 2.5 cm × 2.5 cm, and the effective photovoltaic area, defined by the geometrical overlap between the bottom cathode electrode and the top anode, was 0.09 cm^2. As for the renewal of MoO_3/Al, the electrode of fresh or aged cells was removed by sodium hydroxide solution (0.2 mg/mL). After that, MoO_3 (10 nm) and Al (100 nm) were sequentially vacuum-deposited again according to the standard protocol.

Thin Film Preparation and Characterization. The model thin films for light illumination test were prepared by a spin-coating corresponding solution to cleaned ITO substrates. UV−vis absorption spectrum was measured by a LAMBDA 750 UV/Vis/NIR spectrophotometer (PerkinElmer). X-ray photoelectron spectroscopy (XPS) measurements were performed on a PHI 5000 VersaProbe III. The XPS sample was prepared on a glass substrate of 1 cm × 1 cm that fully cover ITO. The electron spin resonance spectrum (ESR) was detected by EMXplus (Bruker). The samples for ESR measurement were prepared by spin coating P3HT (1000 rpm, 5 mg/mL) and vapor-deposited MoO_3 (5 nm) on a high temperature resistant polyester film (PET) thin film. MoO_3, P3HT, and P3HT/MoO_3 thin films were prepared by the above methods, respectively. Atomic force microscopy (AFM) images of the films were measured with the Park XE-120 microscope using Cr-/Au-coated conducting tips (NSC18,

https://dx.doi.org/10.1021/acsaem.0c01325
ACS Appl. Energy Mater. 2020, 3, 9714−9723

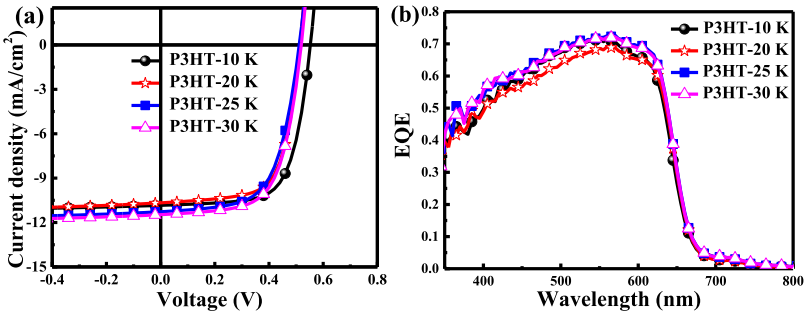

Figure 1. $J-V$ curves (a) and EQE spectra (b) of P3HT:$PC_{61}BM$ cells prepared from P3HT with different polymer molecular weights (10, 20, 25, and 30 K).

MikroMasch, Tallinn, Estonia). Transmission electron microscopy (TEM) images of active layers were obtained using a Tecnai G2 F20 S-Twin 200 kV field-emission electron microscope. The photoactive layers for TEM measurement were prepared by spin-coating the solution onto the cleaned glass substrate, followed by a treatment of Hartree−Fock vapor in the fume hood.

Photovoltaic Performance and Stability Characterizations. PCE of devices was measured in an N_2-filled glove box using a Keithley 2400 source meter under illumination with simulated AM 1.5G sunlight (VeraSol-2, LED 3A Sun simulator, Newport). External quantum efficiency (EQE) spectra were recorded under illumination by a simulated one sun operation condition using bias light from a 532 nm solid-state laser. Light from a 150 W tungsten halogen lamp (Osram 64610) was used as a probe light and was modulated with a mechanical chopper before passing through the monochromator (Zolix, Omni-k300) to select the wavelength. The response was recorded as the voltage by an $I-V$ converter (DNR-IV Convertor, Suzhou D&R Instruments), using a lock-in amplifier (Stanford Research Systems SR 830). A calibrated Si cell was used as a reference. The devices for EQE measurement was kept behind a quartz window in a nitrogen-filled container. The long-term stability of unencapsulated devices was conducted using a multichannel solar cell performance decay test system (PVLT-G8001M, Suzhou D&R Instruments Co. Ltd.) under a testing condition in accordance with ISOS-L-1. The devices were put inside a glove box (H_2O < 1 ppm, O_2 < 1 ppm), and continuously illuminated with white LED light (D&R Light, L-W5300KA-150, Suzhou D&R Instruments). The illumination light intensity was initially set so the output J_{SC} equaled the J_{SC} measured under standard conditions. The illumination light intensity was monitored by a photodiode (Hamamatsu S1336-8BQ). Current−voltage ($J-V$) curves of the devices were checked periodically, and the photovoltaic performance data (V_{OC}, J_{SC}, FF, and PCE) were calculated automatically accordingly to the $J-V$ results. The PCE degradation curves were fitted by gnuplot software (http://www.gnuplot.info/) through the stretched exponential model.[33,34] Highly sensitive EQE curves spectra were measured by a Solar Cell Spectral Response Measurement System PECT-600 (Enlitech, Taiwan, China).

RESULTS AND DISCUSSIONS

Molecular Weight Depended on the Device Performance of P3HT:$PC_{61}BM$ Cells. Regioregular P3HTs with different molecular weights were synthesized by a Ni-catalyzed metathesis coupling reaction.[31] The molecular weight of the polymer was controlled by tuning the feeding ratio of the catalyst to monomer. Four different P3HTs with weight average molecular weight (M_w) of 1.16 × 10^4 g/mol (denoted as P3HT-10 K), 2.12 × 10^4 g/mol (P3HT-20 K), 2.64 × 10^4 g/mol (P3HT-25 K), 3.05 × 10^4 g/mol (P3HT-30 K) were chosen as the polymers for the investigation of molecular weight-dependent degradation behaviors. It is worth noting that all of these polymers have a high regioregularity of 94−97%, which is an important parameter for P3HT materials. Figure 1 shows the $J-V$ curves and EQE spectra of the P3HT:$PC_{61}BM$ cells, and Table 1 lists the photovoltaic performance data. Statistical photovoltaic data are shown in Figure S1 in the Supporting Information. All of these P3HT:$PC_{61}BM$ solar cells show appropriate PCE of 3.5−3.9%, which is comparable to those reported in the literature.[35] V_{OC} of these cells is around 0.51−0.55 V, which is lower than the common value reported in the literature.[36] This could be attributed to the relatively high regioregularity of the synthesized P3HT.[25] J_{SC} of the cells is found to improve with the increase of molecular weight, which can be attributed to the more optimal nanomorphology of the blend film (*vide infra*).[26,37] The photovoltaic performance results shown here indicate that the cells are acceptable for stability comparison after careful optimization.

Degradation Behaviors of the P3HT:$PC_{61}BM$ Cells. Figure 2 shows the evolution of V_{OC}, J_{SC}, FF, and PCE of the P3HT:$PC_{61}BM$ cells aged under simulated operating conditions. Figure S2 in the Supporting Information shows the changes of $J-V$ curves over 400 h. As seen here, all of these cells show fast "burn-in" degradation, and T_{80}, the time the solar cell reaches 80% of initial device performance, is measured to be 22.53, 7.85, 15.73, and 44.55 h for 10, 20, 25, and 30 K P3HT cells, respectively (Table 1). It is worth noting that all of these cells show similar J_{SC} decay rates, independent of the molecular weight of P3HT. Such a fast J_{SC} decay can be attributed to the photon-induced dimerization of $PC_{61}BM$ during aging.[15,16,38] V_{OC} and FF, on the other hand, show a nonmonotonous dependence on the molecular weight of P3HT. The cell based on P3HT-20 K shows the fastest V_{OC} and FF decays, leading to the lowest device performance after aging. PCE after aging for 400 h (PCE^{400}) is only 10% of its initial value, which is much lower than that of the cells based on 10, 25, and 30 K P3HT (38, 43, and 67%). Meanwhile, we performed stretched exponential decay fitting on the PCE decay curves of all devices to further quantitatively describe the decay differences of the four devices. Stretched exponential decay is also called Kohlrausch exponential decay, and is used to describe the decay behaviors of electronic devices with various stress factors.[33,34] The stretched exponential decay is usually described as eq 1,

https://dx.doi.org/10.1021/acsaem.0c01325
ACS Appl. Energy Mater. 2020, 3, 9714−9723

Table 1. Photovoltaic Performance Data of P3HT:$PC_{61}BM$ Cells Prepared from P3HT with Different Molecular Weights (10, 20, 25, and 30 K)

sample	M_w (kg/mol)	M_n (kg/mol)	PDI	Rr (%)	V_{OC} (V)	J_{SC} (mA·cm^2)	FF	PCE (%)	T_{80} (h)[a]	PCE^{400} (%)[b]	PCE (∞)[c]	α[c]	τ (h)[c]	β[c]
P3HT-10 K	11.6	10.1	1.15	94.3	0.55 ± 0.01	10.78 ± 0.10	0.67 ± 0.01	3.97 ± 0.10	22.53	38	0.34	0.71	56.7	0.63
P3HT-20 K	21.2	19.1	1.11	96.1	0.51 ± 0.01	10.56 ± 0.11	0.66 ± 0.01	3.63 ± 0.10	7.85	10	0.11	1.02	23.8	0.67
P3HT-25 K	26.4	18.8	1.40	97.1	0.51 ± 0.00	11.08 ± 0.02	0.62 ± 0.03	3.55 ± 0.07	15.73	43	0.39	0.63	81.2	0.58
P3HT-30 K	30.5	22.3	1.37	97.1	0.52 ± 0.01	11.27 ± 0.20	0.64 ± 0.01	3.75 ± 0.05	44.55	67	0.63	0.38	42.9	0.54

[a]Time that reaches 80% of its initial PCE. [b]The ratio of the PCE aged for 400 h to its initial value (in percentage). [c]Numerical-simulated results obtained by fitting the normalized PCE decay curves to the exponential stretched decay model (eq 1).

$$\mathrm{PCE}(t) = \mathrm{PCE}(\infty) + \alpha \times \exp\left(-\frac{t}{\tau}\right)^{\beta} \quad (1)$$

where τ, α, and PCE (∞) represent the mean lifetime, pre-exponential factor (degradation amplitudes), and the intercept (the saturated PCE over a long time aging), respectively. The stretching exponent β is in the range $0 < \beta \leq 1$. The fitting decay curves are shown in Figure S3, and the corresponding parameters are listed in Table 1. It can be seen that the degradation amplitudes (α) of the four devices were 0.71 (10 K), 1.02 (20 K), 0.63 (25 K), and 0.38 (30 K), respectively, clearly indicating the fastest degradation behavior of P3HT-20 K-based cell. At the same time, the β of P3HT-20 K had the maximum value of 0.67, indicating there is one most prominent decay pathway of this type of cell. The fitted PCE (∞) predicts the final efficiency of the device after long-term aging, which is found to be close to the measured PCE value after aging for 400 h (PCE^{400}, Table 1). The P3HT-20 K-based cell showed a lowest PCE (∞) of 0.11. The mean lifetime τ of the cells were fitted to be 56.7, 23.8, 81.2, and 42.9 h for P3HT-10, 20, 25, and 30 K, respectively, again confirming the lowest stability of the P3HT-20 K cell. It is worth noting that P3HT-30 K showed a lower τ than P3HT-25 K, which is due to the fast decay of J_{SC}, as seen in Figure 2.

Simultaneously, thermal annealing was performed on these aged P3HT:$PC_{61}BM$ cells to check whether such a performance decay is reversible or not. As shown in Figure S4, for the cells with molecular weights of 25 and 30 K, J_{SC} increases slightly after thermal annealing, indicating the partial recovery of J_{SC} decay. However, no noticeable V_{OC} and FF enhancement are found for all of these cells after thermal annealing, indicating the V_{OC} and FF decay of these cells is not fully thermally reversible.

Morphology and Optical Properties of the Blend Films. It was reported that burn-in V_{OC} loss in polymer solar cells is highly dependent on the crystallinity of polymers, where amorphous polymer blend usually leads to fast V_{OC} decay.[18] The crystallinity of the P3HT:$PC_{61}BM$ blends were examined in this work using UV−vis absorption, XRD and TEM. Figures S5a,b and S6 in the Supporting Information show the UV−vis absorption spectra, XRD patterns, and TEM images of P3HT:$PC_{61}BM$ with different P3HTs, respectively. As seen from Figure S5a, all of these films showed broad absorption bands over 300−650 nm, where 0−0 and 0−1 transition absorptions (600 and 570 nm, respectively) can be distinguished, which is ascribed to the intermolecular $\pi-\pi$ stacking of P3HT backbones.[39] The XRD patterns of these films (Figure S5b) showed a diffraction peak at 2θ of 5.57°, corresponding to the lamellar structure of P3HT with an intermolecular distance of 1.57 c5,[40] indicating that all of these P3HT blend films are highly crystalline. The TEM images (Figure S6) of the blend films also confirmed the formation of nanocrystals in these blend films, which is in good accordance with the XRD results. Both the XRD and TEM results demonstrate that all of these P3HT:$PC_{61}BM$ films are highly crystalline, owing to the high regioregularity of the P3HTs (Table 1).

To check the changes in the morphology of these films during aging, UV−vis absorption and EQE spectra of these cells were measured. Figures S7 and S8 in the Supporting Information show the results. As seen in Figure S7, the absorption of crystalline P3HT domains (over 500−650 nm)[39] decreases slightly with less pronounced 0−0 vibration bands,

https://dx.doi.org/10.1021/acsaem.0c01325
ACS Appl. Energy Mater. 2020, 3, 9714−9723

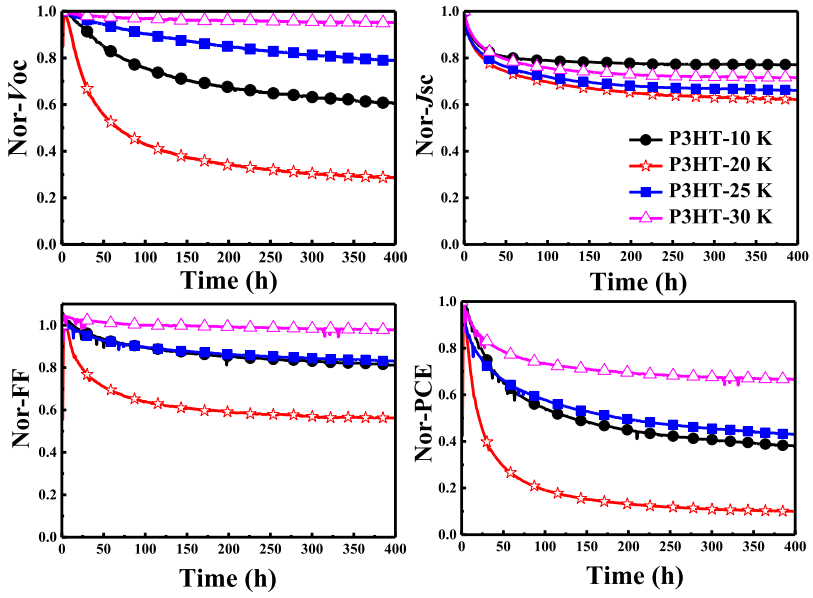

Figure 2. Degradation curves of V_{OC}, J_{SC}, FF, and PCE of the P3HT:$PC_{61}BM$ cells aged under light illumination.

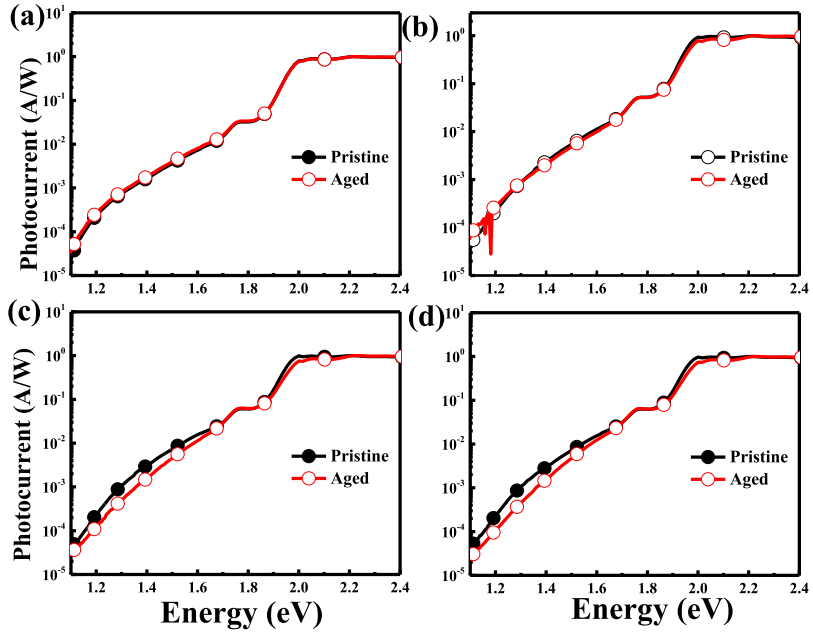

Figure 3. FTPS of the pristine and aged P3HT:$PC_{61}BM$ cells (a) P3HT-10 K, (b) P3HT-20 K, (c) P3HT-25 K, (d) P3HT-30 K.

suggesting the slight decrease of the crystallinity of the P3HT domain during aging, whereas the EQE spectra confirm a similar conclusion (Figure S8). However, there is no direct evidence that P3HT-20 K-based cells showed more significant UV−vis and EQE changes after aging. In other words, there is no direct correlation between the morphology change of the blend film to the fast degradation of the P3HT-20 K-based cell.

Janssen *et al.* reported that the charge transfer state (CT) of the photoactive layer shows a significant influence on the V_{OC} of polymer solar cells.[41] To check whether the CT state of the photoactive layer changes after aging, Fourier transform photocurrent spectroscopy (FTPS) of these cells were measured. Figure 3 shows the results, and the CT state was simulated according to the Marcus theory (see Figure S9 in the Supporting Information).[42] Results indicate that there are no significant changes in the CT state for all of these cells before and after aging. Together with the irreversibility of these cells during aging (*vide supra,* Figure S4), we concluded that the degradation of these cells should not be correlated to the changes in the crystallinity of the P3HT domain.

The surface morphology of the blend films was then measured by AFM. Figure 4 shows the topological AFM images of these films. As seen here, for all of these films rough surfaces are measured with root mean surface roughnesses of 16.9, 28.0, 15.2, and 12.0 nm, respectively. The rough surface could be due to the high crystallinity of these P3HTs. Interestingly, the film made of P3HT-20 K has the largest roughness, which will increase the interface connection between P3HT and the thermally evaporated MoO_3 layer. Because the open circuit voltage of polymer solar cells is highly sensitive to the interfacial charge recombination, we, therefore,

https://dx.doi.org/10.1021/acsaem.0c01325
ACS Appl. Energy Mater. 2020, 3, 9714−9723

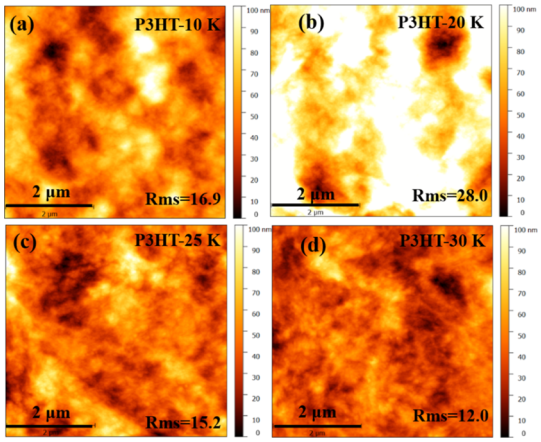

Figure 4. AFM topological image of P3HT:$PC_{61}BM$ films with different P3HT molecular weights [(a) P3HT-10 K, (b) P3HT-20 K, (c) P3HT-25 K, (d) P3HT-30 K].

speculate that interfacial degradation could be the main reason for the performance decay of this type of cell.

V_{OC} and FF Recovery After Renewing the MoO_3/Al Electrode. To further confirm that interfacial degradation is the main reason causes the fast V_{OC} and FF decay of these cells, we renewed the MoO_3/Al electrode of the aged cells and tested the performance of the cells. By using dilute NaOH solution, we are able to remove the MoO_3/Al electrode of the cells without influencing the photoactive layer.[16] Figure 5 shows the $J-V$ curves of pristine cells, aged cells, and the aged cells with the renewed MoO_3/Al electrode, and the photovoltaic performance data are listed in Table S1 in the Supporting Information. In all cells with different P3HT, J_{SC} is not recovered after renewing the top electrode. However, both V_{OC} and FF increase with the renewed MoO_3/Al electrode. For example, the V_{OC} of aged P3HT-20 K cells is 0.28 V, which increases to 0.50 V after renewing the MoO_3/Al electrode, close to that of the fresh cell (0.52 V). These results unambiguously confirm that interfacial degradation is the main reason for the V_{OC} and FF decay of cells. It is known that the P3HT-20 K/$PC_{61}BM$ has a rougher surface than other P3HTs, which increases the interconnection between P3HT and MoO_3 and consequently enhances the interfacial photon chemical reaction. These results are well-corresponding to the fastest V_{OC} and FF decay of the P3HT-20 K-based cells.

Interfacial Photoreduction of MoO_3 by P3HT. To understand the photochemical reaction of the interface of the cell during aging, we fabricated and tested the chemical changes of the P3HT (15 nm)/MoO_3 (5 nm), $PC_{61}BM$ (15 nm)/MoO_3 (5 nm), and P3HT:$PC_{61}BM$ (15 nm)/MoO_3 (5 nm) films, where P3HT-20 K was used as the polymer and the films were aged under white light (using the same light source for the solar cell aging test). For comparison, reference MoO_3, P3HT, and $PC_{61}BM$ films on ITO glass were also made and tested. The UV−vis absorption spectra of these films illuminated at different times are shown in Figures 6 and S10. As seen from Figure S10a−c, no obvious absorption changes can be detected for MoO_3, $PC_{61}BM$, and $PC_{61}BM$/MoO_3 films, suggesting that properties of these three films do not change under light illumination. In contrast, for P3HT:$PC_{61}BM$/MoO_3 and P3HT/MoO_3 films (Figure 6a,b), absorption enhancement over 400−650 nm can be clearly seen. Note that both pure P3HT and P3HT:PCBM films on ITO glass show almost no absorption change under light illumination (Figure 6c and S10d), and all of these samples are placed onto a cold plate with a temperature of 25 °C, such an absorption enhancement cannot be attributed to the increase of the crystallinity of P3HT as a result of the heating effect of light illumination. Also note that no obvious absorption change for the P3HT/MoO_3 film kept in the dark was observed (Figure S10e). In contrast, the enhancement of absorption for the P3HT:$PC_{61}BM$/MoO_3 and P3HT/MoO_3 indicates that there is an intensive interaction between P3HT and MoO_3 under light illumination. Figure S11 in the Supporting Information shows the absorption spectra of P3HT:$PC_{61}BM$ and P3HT films with different molecular weights under light illumination. Both the films with or/without the MoO_3 layer were measured. Similar to P3HT-20 K-based films, no obvious absorption change was observed for all films without the MoO_3 layer under light illumination. In contrast, films with the MoO_3 layer show characteristic absorption enhancement over 400−650 nm, confirming the

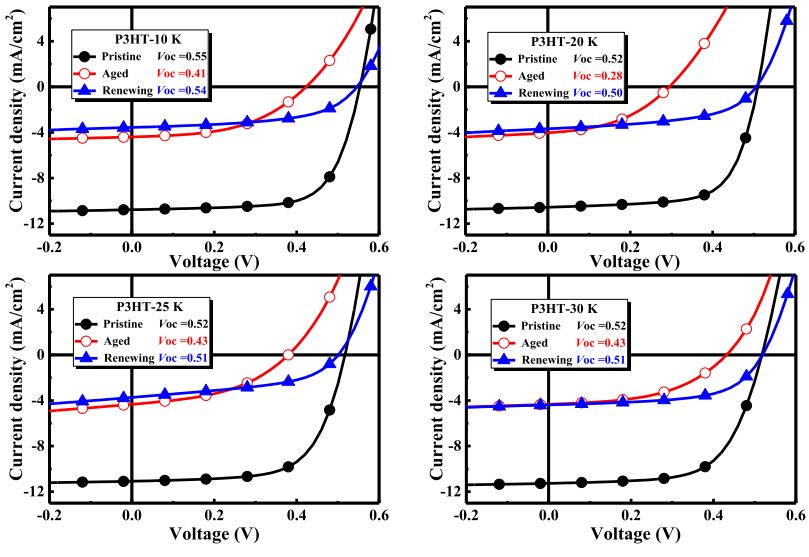

Figure 5. $J-V$ curves of pristine cells, aged cells, and the aged cells with renewed MoO_3/Al electrodes.

https://dx.doi.org/10.1021/acsaem.0c01325
ACS Appl. Energy Mater. 2020, 3, 9714−9723

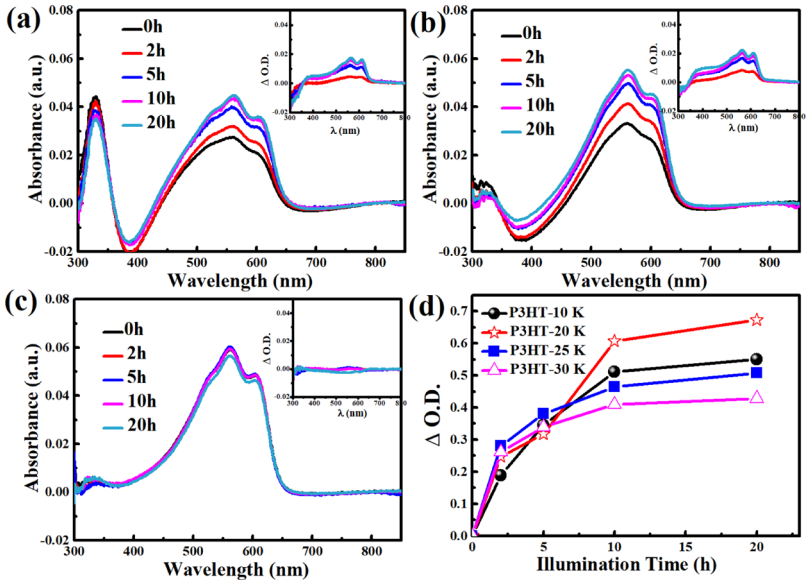

Figure 6. UV−vis absorption spectra of P3HT-20 K/PCBM/MoO_3 (a), P3HT-20 K/MoO_3 (b), and P3HT (c) films illuminated with LED white light for different hours (at 25 °C); the insertion is the optical density difference for the films after illuminated with light for different times; (d) absorbance changes at 560 nm for different P3HT illuminated under light for a certain time.

generality of such a photon chemical interaction between P3HT and MoO_3. The absorption enhancement over the illumination time for different P3HT is plotted and shown in Figure 6d. As seen here, P3HT-20 K shows a much faster absorption enhancement than other P3HTs, which is in good accordance with the device stability of the P3HT-based cells (Figure 2), further confirming that interfacial PCR of MoO_3 by P3HT should be the main reason for the fast V_{OC} and FF decay of P3HT-20 K cells.

Such a chemical reaction between P3HT and MoO_3 can also be found in the solution. Figure S12 in the Supporting Information shows the optical images of the P3HT (in chlorobenzene)/MoO_3 (in water) biphasic solution under light illumination. As clearly shown here, color of the P3HT solution turned darker with the increase of illumination time. The UV−vis absorption spectra of the P3HT solution taken with a syringe was measured, and results showed a dramatic enhancement in absorption over 350−550 nm, corresponding very well to that of the thin film under light illumination (Figure 6a,b). It was reported that the oxidization of P3HT would lead to the formation of the quinoid structure of the P3HT backbone, which will enhance the $\pi-\pi$ interaction between P3HT chains and consequently increase the 0−0 transition absorption.[39,43] Photon-induced electron transfer from P3HT to MoO_3 is then proposed to be the main chemical reaction between these two components.

To further understand the chemical interaction between the photoactive layer and the MoO_3/Al electrode, ESR of the thin films of MoO_3, P3HT-20 K, and P3HT-20 K/MoO_3 were measured. The experimental results are shown in Figure 7. As seen here, no ESR signal was measured for MoO_3 and P3HT-20 K films, while a weak but obvious ESR signal ascribed to P3HT polarons was detected for the P3HT/MoO_3 film. The origin of the signal can be attributed to the CT between P3HT and hole-extraction layer MoO_3 under dark conditions.[44,45] Under light illumination, the P3HT film showed an ESR peak with a g value of 2.0023, which increases slightly with the increase of light illumination time. This resonance peak was attributed to the P3HT polaron originating from the oxidation

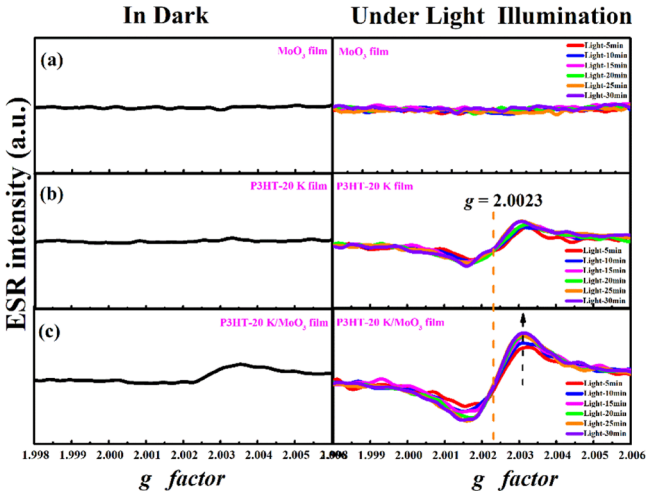

Figure 7. ESR spectra of MoO_3 (a), P3HT-20 K (b), and P3HT-20 K/MoO_3 (c) films in dark and in light measured at 123 K.

of P3HT by residual oxygen.[45−47] For the P3HT/MoO_3 film, more intensive ESR signal was measured than the P3HT film. Note that all of these samples were prepared by spin-coating P3HT onto the PET substrate under identical conditions. The higher ESR signal for the P3HT/MoO_3 film indicated a higher P3HT polaron concentration, which is proposed to be due to the oxidation of P3HT by MoO_3 under light illumination. In addition, this polaron signal increases with the increase of light illumination time, confirming that light illumination can promote the oxidation of P3HT by MoO_3. The signal of MoO_3 was found to be much lower than that of the P3HT polaron. Only a weak Mo(V) signal can be measured even when a high microwave power was applied (Figure S13 in the Supporting Information). The weak ESR signal of MoO_3 may be ascribed to short spin−lattice relaxation time because of heavy element at high temperatures.[47]

To further understand the chemical reaction between MoO_3 and P3HT, the P3HT-20 K (15 nm)/MoO_3 (5 nm) film was

https://dx.doi.org/10.1021/acsaem.0c01325
ACS Appl. Energy Mater. 2020, 3, 9714−9723

illuminated with light for different times, and the films were then checked with XPS. Figure 8 shows the XPS of Mo 3d of

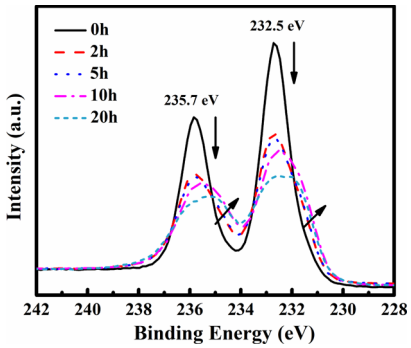

Figure 8. XPS spectra of Mo of P3HT/MoO_3 films under light illumination for different times.

the films with different illumination times. For a fresh P3HT/MoO_3 film, two typical peaks at 232.5 and 235.7 eV were measured, which can be attributed to the signals of Mo^{6+}.[48] With the increase of light illumination time, the XPS peaks turn to be broader and less intensive. By peak fitting (see Figure S14 in the Supporting Information), two sets of peaks with the value of 232.5/235.7 eV and 231.4/234.6 eV can be deduced, which can be attributed to the signal of Mo^{6+} and Mo^{5+}, respectively. This result indicates that Mo(VI) is partially reduced to Mo(V) by P3HT under light illumination. In combination with the ESR results, one can conclude that photo−redox reaction occurs between P3HT and MoO_3 with the increase of light time, which leads to the increase of the absorption of P3HT/MoO_3 films.

With that, an interfacial photochemical reaction between P3HT and MoO_3 is then proposed as shown in Figure 9,

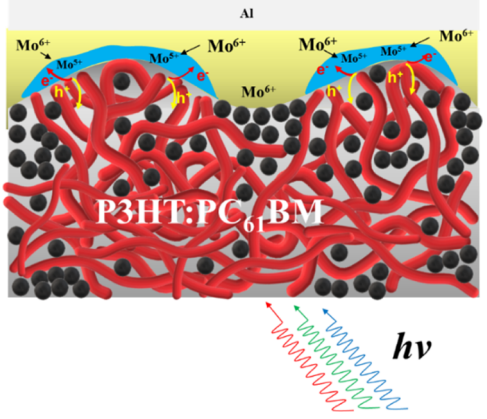

Figure 9. Interfacial PCR of MoO_3 by P3HT that causes fast V_{OC} and FF decay of the cell.

where the direct connection of P3HT with MoO_3 leads to the formation of Mo(V) under light illumination, which increases interfacial charge recombination and consequently reduces the V_{OC} and FF of the cells.[49−51] These results suggest that new interfacial materials that do not react with conjugated polymer highly need to achieve highly stable polymer solar cells.

CONCLUSIONS

In summary, we have clearly demonstrated the interfacial photochemical reaction of P3HT and MoO_3 by the enhanced UV−vis absorption over 400−650 nm, the increased P3HT polaron ESR signal and the transformation of Mo(VI) to Mo(V) in XPS results. Such an interfacial photochemical reaction was then correlated to the fast V_{OC} and FF decays of the P3HT:PC_{61}BM cells because both V_{OC} and FF were recovered for the aged cells after renewing the MoO_3/Al electrode. For the first time, we demonstrated a new interfacial degradation pathway for polymer solar cells that p-type conjugated polymer might react with the p-type metal oxide under light illumination. In addition, the performance decay behaviors of the cells are found to be molecular weight related, which is finally ascribed to the different surface morphologies of the final photoactive layer, which is further supported by the faster enhancement of UV−vis absorption over 400−650 nm.

ASSOCIATED CONTENT

Supporting Information

The Supporting Information is available free of charge at https://pubs.acs.org/doi/10.1021/acsaem.0c01325.

J−*V* curves, EQE spectra, statistical data, FTPS and degradation curves of solar cells before and after aged, UV−vis spectra, XRD patterns, TEM images, ESR spectra, and XPS spectra of different films (PDF)

AUTHOR INFORMATION

Corresponding Authors

Yongzhen Yang − *Key Laboratory of Interface Science and Engineering in Advanced Materials, Ministry of Education, Taiyuan University of Technology, Taiyuan 030024, P. R. China;* orcid.org/0000-0003-0566-4802; Email: yyztyut@126.com

Chang-Qi Ma − *Printable Electronics Research Center, Suzhou Institute of Nano-Tech and Nano-Bionic, Chinese Academy of Sciences (CAS), Suzhou 215123, P. R. China;* orcid.org/0000-0002-9293-5027; Email: cqma2011@sinano.ac.cn

Authors

Huimin Gu − *Key Laboratory of Interface Science and Engineering in Advanced Materials, Ministry of Education, Taiyuan University of Technology, Taiyuan 030024, P. R. China; Printable Electronics Research Center, Suzhou Institute of Nano-Tech and Nano-Bionic, Chinese Academy of Sciences (CAS), Suzhou 215123, P. R. China*

Lingpeng Yan − *Printable Electronics Research Center, Suzhou Institute of Nano-Tech and Nano-Bionic, Chinese Academy of Sciences (CAS), Suzhou 215123, P. R. China; Institute of New Carbon Materials, Taiyuan University of Technology, Taiyuan 030024, P. R. China*

Sonam Saxena − *ARC Centre of Excellence in Exciton Science, School of Chemistry, Bio21 Institute, University of Melbourne, Parkville, Victoria 3010, Australia*

Xueliang Shi − *Shanghai Key Laboratory of Green Chemistry and Chemical Processes, School of Chemistry and Molecular Engineering, East China Normal University, Shanghai 200062, China*

Xuning Zhang − *CAS Key Laboratory of Nanosystem and Hierarchical Fabrication, CAS Center for Excellence in Nanoscience, National Center for Nanoscience and Technology, Beijing 100190, China; School of Chemistry, Beijing Advanced Innovation Center for Biomedical Engineering, Beihang University, Beijing 100191, P. R. China*

https://dx.doi.org/10.1021/acsaem.0c01325
ACS Appl. Energy Mater. 2020, 3, 9714−9723

Zerui Li − *Printable Electronics Research Center, Suzhou Institute of Nano-Tech and Nano-Bionic, Chinese Academy of Sciences (CAS), Suzhou 215123, P. R. China*

Qun Luo − *Printable Electronics Research Center, Suzhou Institute of Nano-Tech and Nano-Bionic, Chinese Academy of Sciences (CAS), Suzhou 215123, P. R. China;* orcid.org/0000-0002-7527-460X

Huiqiong Zhou − *CAS Key Laboratory of Nanosystem and Hierarchical Fabrication, CAS Center for Excellence in Nanoscience, National Center for Nanoscience and Technology, Beijing 100190, China;* orcid.org/0000-0003-2124-6563

Xuguang Liu − *Key Laboratory of Interface Science and Engineering in Advanced Materials, Ministry of Education and Institute of New Carbon Materials, Taiyuan University of Technology, Taiyuan 030024, P. R. China*

Wallace W. H. Wong − *ARC Centre of Excellence in Exciton Science, School of Chemistry, Bio21 Institute, University of Melbourne, Parkville, Victoria 3010, Australia;* orcid.org/0000-0001-7131-8532

Complete contact information is available at: https://pubs.acs.org/10.1021/acsaem.0c01325

Notes

The authors declare no competing financial interest.

■ ACKNOWLEDGMENTS

The authors would like to acknowledge the financial support from the Ministry of Science and Technology of China (no. 2016YFA0200700), the Chinese Academy of Science (no. YJKYYQ20180029 and CAS-ITRI 2019010), the National Natural Science Foundation of China (61904121), the Youth Innovation Promotion Association, CAS (2019317), and the support of Suzhou Vacuum Interconnected Nanotechnology Workstation H005-2019 project. WWHW and SS are supported by the Australian Renewable Energy Agency through the Australian Centre for Advanced Photovoltaics as well as the ARC Centre of Excellence in Exciton Science (CE170100026).

■ REFERENCES

(1) Krebs, F. C.; Espinosa, N.; Hösel, M.; Søndergaard, R. R.; Jørgensen, M. 25th anniversary article: rise to power−OPV-based solar parks. *Adv. Mater.* **2014**, *26*, 29−39.

(2) Hou, J.; Inganäs, O.; Friend, R. H.; Gao, F. Organic solar cells based on non-fullerene acceptors. *Nat. Mater.* **2018**, *17*, 119−128.

(3) Lu, L.; Zheng, T.; Wu, Q.; Schneider, A. M.; Zhao, D.; Yu, L. Recent advances in bulk heterojunction polymer solar cells. *Chem. Rev.* **2015**, *115*, 12666−12731.

(4) Yan, T.; Song, W.; Huang, J.; Peng, R.; Huang, L.; Ge, Z. 16.67% rigid and 14.06% flexible organic solar cells enabled by ternary heterojunction strategy. *Adv. Mater.* **2019**, *31*, 1902210.

(5) Cui, Y.; Yao, H.; Zhang, J.; Zhang, T.; Wang, Y.; Hong, L.; Xian, K.; Xu, B.; Zhang, S.; Peng, J. Over 16% efficiency organic photovoltaic cells enabled by a chlorinated acceptor with increased open-circuit voltages. *Nat. Commun.* **2019**, *10*, 2515.

(6) Lin, Y.; Adilbekova, B.; Firdaus, Y.; Yengel, E.; Faber, H.; Sajjad, M.; Zheng, X.; Yarali, E.; Seitkhan, A.; Bakr, O. M. 17% efficient organic solar cells based on liquid exfoliated WS_2 as a replacement for PEDOT: PSS. *Adv. Mater.* **2019**, *31*, 1902965.

(7) Meng, L.; Zhang, Y.; Wan, X.; Li, C.; Zhang, X.; Wang, Y.; Ke, X.; Xiao, Z.; Ding, L.; Xia, R.; Yip, H.-L.; Cao, Y.; Chen, Y. Organic and solution-processed tandem solar cells with 17.3% efficiency. *Science* **2018**, *361*, 1094−1098.

(8) Du, X.; Heumueller, T.; Gruber, W.; Classen, A.; Unruh, T.; Li, N.; Brabec, C. J. Efficient polymer solar cells based on non-fullerene acceptors with potential device lifetime approaching 10 years. *Joule* **2019**, *3*, 215−226.

(9) Mateker, W. R.; Sachs-Quintana, I. T.; Burkhard, G. F.; Cheacharoen, R.; McGehee, M. D. Minimal long-term intrinsic degradation observed in a polymer solar cell illuminated in an oxygen-free environment. *Chem. Mater.* **2015**, *27*, 404−407.

(10) Martynov, I. V.; Akkuratov, A. V.; Luchkin, S. Y.; Tsarev, S. A.; Babenko, S. D.; Petrov, V. G.; Stevenson, K. J.; Troshin, P. A. Impressive radiation stability of organic solar cells based on fullerene derivatives and carbazole-containing conjugated polymers. *ACS Appl. Mater. Interfaces* **2019**, *11*, 21741−21748.

(11) Gevorgyan, S. A.; Espinosa, N.; Ciammaruchi, L.; Roth, B.; Livi, F.; Tsopanidis, S.; Züfle, S.; Queirós, S.; Gregori, A.; dos Reis Benatto, G. A.; Corazza, M.; Madsen, M. V.; Hösel, M.; Beliatis, M. J.; Larsen-Olsen, T. T.; Pastorelli, F.; Castro, A.; Mingorance, A.; Lenzi, V.; Fluhr, D.; Roesch, R.; Maria Duarte Ramos, M.; Savva, A.; Hoppe, H.; Marques, L. S. A.; Burgués, I.; Georgiou, E.; Serrano-Luján, L.; Krebs, F. C. Baselines for lifetime of organic solar cells. *Adv. Energy Mater.* **2016**, *6*, 1600910.

(12) Peters, C. H.; Sachs-Quintana, I. T.; Mateker, W. R.; Heumueller, T.; Rivnay, J.; Noriega, R.; Beiley, Z. M.; Hoke, E. T.; Salleo, A.; McGehee, M. D. The mechanism of burn-in loss in a high efficiency polymer solar cell. *Adv. Mater.* **2012**, *24*, 663−668.

(13) Reese, M. O.; Nardes, A. M.; Rupert, B. L.; Larsen, R. E.; Olson, D. C.; Lloyd, M. T.; Shaheen, S. E.; Ginley, D. S.; Rumbles, G.; Kopidakis, N. Photoinduced degradation of polymer and polymer−fullerene active layers: experiment and theory. *Adv. Funct. Mater.* **2010**, *20*, 3476−3483.

(14) Distler, A.; Sauermann, T.; Egelhaaf, H.-J.; Rodman, S.; Waller, D.; Cheon, K.-S.; Lee, M.; Guldi, D. M. The effect of PCBM dimerization on the performance of bulk heterojunction solar cells. *Adv. Energy Mater.* **2014**, *4*, 1300693.

(15) Heumueller, T.; Mateker, W. R.; Distler, A.; Fritze, U. F.; Cheacharoen, R.; Nguyen, W. H.; Biele, M.; Salvador, M.; von Delius, M.; Egelhaaf, H.-J.; McGehee, M. D.; Brabec, C. J. Morphological and electrical control of fullerene dimerization determines organic photovoltaic stability. *Energy Environ. Sci.* **2016**, *9*, 247−256.

(16) Yan, L.; Yi, J.; Chen, Q.; Dou, J.; Yang, Y.; Liu, X.; Chen, L.; Ma, C.-Q. External load-dependent degradation of P3HT:$PC_{61}BM$ solar cells: behavior, mechanism, and method of suppression. *J. Mater. Chem. A* **2017**, *5*, 10010−10020.

(17) Heumueller, T.; Burke, T. M.; Mateker, W. R.; Sachs-Quintana, I. T.; Vandewal, K.; Brabec, C. J.; McGehee, M. D. Disorder-induced open-circuit voltage losses in organic solar cells during photoinduced burn-in. *Adv. Energy Mater.* **2015**, *5*, 1500111.

(18) Heumueller, T.; Mateker, W. R.; Sachs-Quintana, I. T.; Vandewal, K.; Bartelt, J. A.; Burke, T. M.; Ameri, T.; Brabec, C. J.; McGehee, M. D. Reducing burn-in voltage loss in polymer solar cells by increasing the polymer crystallinity. *Energy Environ. Sci.* **2014**, *7*, 2974−2980.

(19) Li, N.; Perea, J. D.; Kassar, T.; Richter, M.; Heumueller, T.; Matt, G. J.; Hou, Y.; Güldal, N. S.; Chen, H.; Chen, S.; Langner, S.; Berlinghof, M.; Unruh, T.; Brabec, C. J. Abnormal strong burn-in degradation of highly efficient polymer solar cells caused by spinodal donor-acceptor demixing. *Nat. Commun.* **2017**, *8*, 14541.

(20) Sachs-Quintana, I.; Heumüller, T.; Mateker, W. R.; Orozco, D. E.; Cheacharoen, R.; Sweetnam, S.; Brabec, C. J.; McGehee, M. D. Electron barrier formation at the organic-back contact interface is the first step in thermal degradation of polymer solar cells. *Adv. Funct. Mater.* **2014**, *24*, 3978−3985.

(21) Jiang, Y.; Sun, L.; Jiang, F.; Xie, C.; Hu, L.; Dong, X.; Qin, F.; Liu, T.; Hu, L.; Jiang, X.; Zhou, Y. Photocatalytic effect of ZnO on the stability of nonfullerene acceptors and its mitigation by SnO_2 for nonfullerene organic solar cells. *Mater. Horiz.* **2019**, *6*, 1438−1443.

(22) Park, S.; Son, H. J. Intrinsic photo-degradation and mechanism of polymer solar cells: the crucial role of non-fullerene acceptors. *J. Mater. Chem. A* **2019**, *7*, 25830−25837.

(23) Yan, L.; Gu, H.; Li, Z.; Zhang, J.; Yang, Y.; Wang, H.; Liu, X.; Wei, Z.; Luo, Q.; Ma, C.-Q. The interfacial degradation mechanism of polymer:fullerene bis-adduct solar cells and their stability improvement. *Adv. Mater.* **2020**, *1*, 1307−1317.
(24) Woo, C. H.; Thompson, B. C.; Kim, B. J.; Toney, M. F.; Fréchet, J. M. J. The influence of poly (3-hexylthiophene) regioregularity on fullerene-composite solar cell performance. *J. Am. Chem. Soc.* **2008**, *130*, 16324−16329.
(25) Chandrasekaran, N.; Liu, A. C. Y.; Kumar, A.; McNeill, C. R.; Kabra, D. Effect of regioregularity on recombination dynamics in inverted bulk heterojunction organic solar cells. *J. Phys. D: Appl. Phys.* **2017**, *51*, 015501.
(26) Schilinsky, P.; Asawapirom, U.; Scherf, U.; Biele, M.; Brabec, C. J. Influence of the molecular weight of poly (3-hexylthiophene) on the performance of bulk heterojunction solar cells. *Chem. Mater.* **2005**, *17*, 2175−2180.
(27) Osaka, I.; Saito, M.; Mori, H.; Koganezawa, T.; Takimiya, K. Drastic change of molecular orientation in a thiazolothiazole copolymer by molecular-weight control and blending with $PC_{61}BM$ leads to high efficiencies in solar cells. *Adv. Mater.* **2012**, *24*, 425−430.
(28) Subbiah, J.; Purushothaman, B.; Chen, M.; Qin, T.; Gao, M.; Vak, D.; Scholes, F. H.; Chen, X.; Watkins, S. E.; Wilson, G. J.; Holmes, A. B.; Wong, W. W.; Jones, D. J. Organic solar cells using a high-molecular-weight benzodithiophene−benzothiadiazole copolymer with an efficiency of 9.4%. *Adv. Mater.* **2015**, *27*, 702−705.
(29) Li, W.; Yang, L.; Tumbleston, J. R.; Yan, L.; Ade, H.; You, W. Controlling molecular weight of a high efficiency donor-acceptor conjugated polymer and understanding its significant impact on photovoltaic properties. *Adv. Mater.* **2014**, *26*, 4456−4462.
(30) Hiorns, R. C.; de Bettignies, R.; Leroy, J.; Bailly, S.; Firon, M.; Sentein, C.; Khoukh, A.; Preud'homme, H.; Dagron-Lartigau, C. High molecular weights, polydispersities, and annealing temperatures in the optimization of bulk-heterojunction photovoltaic cells based on poly (3-hexylthiophene) or poly (3-butylthiophene). *Adv. Funct. Mater.* **2006**, *16*, 2263−2273.
(31) Loewe, R. S.; Khersonsky, S. M.; McCullough, R. D. A simple method to prepare head-to-tail coupled, regioregular poly (3-alkylthiophenes) using Grignard metathesis. *Adv. Mater.* **1999**, *11*, 250−253.
(32) Beek, W. J. E.; Wienk, M. M.; Kemerink, M.; Yang, X.; Janssen, R. A. J. Hybrid zinc oxide conjugated polymer bulk heterojunction solar cells. *J. Phys. Chem. B* **2005**, *109*, 9505−9516.
(33) Berberan-Santos, M. N.; Bodunov, E. N.; Valeur, B. Mathematical functions for the analysis of luminescence decays with underlying distributions 1. Kohlrausch decay function (stretched exponential). *Chem. Phys.* **2005**, *315*, 171−182.
(34) Johnston, D. C. Stretched exponential relaxation arising from a continuous sum of exponential decays. *Phys. Rev. B* **2006**, *74*, 184430.
(35) Dang, M. T.; Hirsch, L.; Wantz, G. P3HT: PCBM, best seller in polymer photovoltaic research. *Adv. Mater.* **2011**, *23*, 3597−3602.
(36) Li, G.; Shrotriya, V.; Huang, J.; Yao, Y.; Moriarty, T.; Emery, K.; Yang, Y. *High-Efficiency Solution Processable Polymer Photovoltaic Cells by Self-Organization of Polymer Blends*; World Scientific, 2011; pp 80−84.
(37) Liu, F.; Chen, D.; Wang, C.; Luo, K.; Gu, W.; Briseno, A. L.; Hsu, J. W. P.; Russell, T. P. Molecular weight dependence of the morphology in P3HT: PCBM solar cells. *ACS Appl. Mater. Interfaces* **2014**, *6*, 19876−19887.
(38) Yan, L.; Wang, Y.; Wei, J.; Ji, G.; Gu, H.; Li, Z.; Zhang, J.; Luo, Q.; Wang, Z.; Liu, X.; Xu, B.; Wei, Z.; Ma, C.-Q. Simultaneous performance and stability improvement of polymer: fullerene solar cells by doping with piperazine. *J. Mater. Chem. A* **2019**, *7*, 7099−7108.
(39) Ehrenreich, P.; Birkhold, S. T.; Zimmermann, E.; Hu, H.; Kim, K.-D.; Weickert, J.; Pfadler, T.; Schmidt-Mende, L. H-aggregate analysis of P3HT thin films-Capability and limitation of photoluminescence and UV/Vis spectroscopy. *Sci. Rep.* **2016**, *6*, 32434.
(40) Noguchi, Y.; Saeki, A.; Fujiwara, T.; Yamanaka, S.; Kumano, M.; Sakurai, T.; Matsuyama, N.; Nakano, M.; Hirao, N.; Ohishi, Y.; Seki, S. Pressure modulation of backbone conformation and intermolecular distance of conjugated polymers toward understanding the dynamism of π-figuration of their conjugated system. *J. Phys. Chem. B* **2015**, *119*, 7219−7230.
(41) Veldman, D.; Meskers, S. C. J.; Janssen, R. A. J. The energy of charge-transfer states in electron donor−acceptor blends: insight into the energy losses in organic solar cells. *Adv. Funct. Mater.* **2009**, *19*, 1939−1948.
(42) Vandewal, K.; Tvingstedt, K.; Gadisa, A.; Inganäs, O.; Manca, J. V. Relating the open-circuit voltage to interface molecular properties of donor: acceptor bulk heterojunction solar cells. *Phys. Rev. B* **2010**, *81*, 125204.
(43) Nia, N. Y.; Lamanna, E.; Zendehdel, M.; Palma, A. L.; Zurlo, F.; Castriotta, L. A.; Di Carlo, A. Doping strategy for efficient and stable triple cation hybrid perovskite solar cells and module based on poly (3-hexylthiophene) hole transport layer. *Small* **2019**, *15*, 1904399.
(44) Marumoto, K.; Fujimori, T.; Ito, M.; Mori, T. Charge formation in pentacene layers during solar-cell fabrication: direct observation by electron spin resonance. *Adv. Energy Mater.* **2012**, *2*, 591−597.
(45) Nagamori, T.; Marumoto, K. Direct observation of hole accumulation in polymer solar cells during device operation using light-induced electron spin resonance. *Adv. Mater.* **2013**, *25*, 2362−2367.
(46) Havlicek, M.; Sariciftci, N. S.; Scharber, M. C. Degradation kinetics in different polymer−fullerene blends investigated by electron spin resonance. *J. Mater. Res.* **2018**, *33*, 1853−1859.
(47) Son, D.; Kuwabara, T.; Takahashi, K.; Marumoto, K. Direct observation of UV-induced charge accumulation in inverted-type polymer solar cells with a TiO_x layer: microscopic elucidation of the light-soaking phenomenon. *Appl. Phys. Lett.* **2016**, *109*, 133301.
(48) He, T.; Yao, J. Photochromism of molybdenum oxide. *J. Photochem. Photobiol., C* **2003**, *4*, 125−143.
(49) Zhang, H.; Borgschulte, A.; Castro, F. A.; Crockett, R.; Gerecke, A. C.; Deniz, O.; Heier, J.; Jenatsch, S.; Nüesch, F.; Sanchez-Sanchez, C.; Zoladek-Lemanczyk, A.; Hany, R. Photochemical transformations in fullerene and molybdenum oxide affect the stability of bilayer organic solar cells. *Adv. Energy Mater.* **2015**, *5*, 1400734.
(50) Huang, P.-H.; Huang, C.-J.; Chen, K.-L.; Ke, J.-C.; Wang, Y.-H.; Kang, C.-C. Improved reliability of small molecule organic solar cells by double anode buffer layers. *J. Nanomater.* **2014**, *2014*, 1−6.
(51) Li, Z.; Liu, C.; Guo, J.; Zhang, X.; Zhou, Y.; Shen, L.; Guo, W. Reducing charge recombination of polymer solar cells by introducing composite anode buffer layer. *Sol. Energy* **2018**, *171*, 8−15.

https://dx.doi.org/10.1021/acsaem.0c01325
ACS Appl. Energy Mater. 2020, 3, 9714−9723